Spectroscopic studies of surface–gas interactions and catalyst restructuring at ambient pressure: mind the gap!

2008 J. Phys.: Condens. Matter 20 184019

(http://iopscience.iop.org/0953-8984/20/18/184019)

J. Phys.: Condens. Matter **20** (2008) 184019 (17pp) doi:10.1088/0953-8984/20/18/184019

Spectroscopic studies of surface–gas interactions and catalyst restructuring at ambient pressure: mind the gap!

Günther Rupprechter[1] **and Christian Weilach**

Institute of Materials Chemistry, Vienna University of Technology, Veterinärplatz 1, A-1210 Vienna, Austria

E-mail: grupp@imc.tuwien.ac.at

Received 23 October 2007, in final form 7 December 2007
Published 17 April 2008
Online at stacks.iop.org/JPhysCM/20/184019

Abstract

Recent progress in the application of surface vibrational spectroscopy at ambient pressure allows us to monitor surface–gas interactions and heterogeneous catalytic reactions under conditions approaching those of technical catalysis. The surface specificity of photon-based methods such as polarization modulation infrared reflection absorption spectroscopy (PM-IRAS) and sum frequency generation (SFG) spectroscopy is utilized to monitor catalytically active surfaces while they function at high pressure and high temperature. Together with complementary information from high-pressure x-ray photoelectron spectroscopy (HP-XPS) and high-resolution transmission electron microscopy (HRTEM), reaction mechanisms can be deduced on a molecular level. Well defined model catalysts, prepared under ultrahigh vacuum (UHV), are typically employed in such studies, including smooth and stepped single crystals, thin oxide films, and oxide-supported nanoparticles.

A number of studies on unsupported and supported noble metal (Pd, Rh) catalysts are presented, focusing on the transformation of the catalysts from the 'as-prepared' to the 'active state'. This often involves pronounced alterations in catalyst structure and composition, for example the creation of surface carbon phases, surface oxides or surface alloys, as well as nanoparticle restructuring. The reactivity studies include CH_3OH, CH_4 and CO oxidation with gas phase analysis by gas chromatography and mass spectrometry. Differing results between studies under ultrahigh vacuum and ambient pressure, and between studies on single crystals and supported nanoparticles, demonstrate the importance of 'minding the gap' between idealized and realistic conditions.

(Some figures in this article are in colour only in the electronic version)

1. A new twist to an old story?

The transformation of a heterogeneous catalyst from the 'as-prepared' to the 'active state', which may involve pronounced changes in catalyst structure and composition, is a traditional topic of catalysis research [1–19]. Scientists soon realized that a number of effects may occur during the activation, lifetime and regeneration of an oxide supported metal catalyst (for example, Pd–Al_2O_3) (figure 1):

(i) *Nanoparticle restructuring.* Sequences of oxidation and reduction at temperatures up to ∼773 K, frequently utilized to activate or rejuvenate a catalyst, not only remove synthesis residues and contaminants but may also lead to sintering (figure 1(a)) or redispersion of the metal nanoparticles [20]. Even when changes in particle size (dispersion) are absent, alterations of the particle shape and surface structure (reshaping, restructuring) have frequently been reported [1–22]. Such changes depend on the relative surface energies of metal, metal oxide and support oxide (wetting and de-wetting behavior) and can favor low-index (smooth) or high-index (rough) surfaces (figure 1(b)) [18]. The changes in surface energy are induced by gas (O_2, H_2) adsorption, the removal of contaminants or partial reduction of the support oxide (metal–support interaction [21, 22]).

[1] Author to whom any correspondence should be addressed.

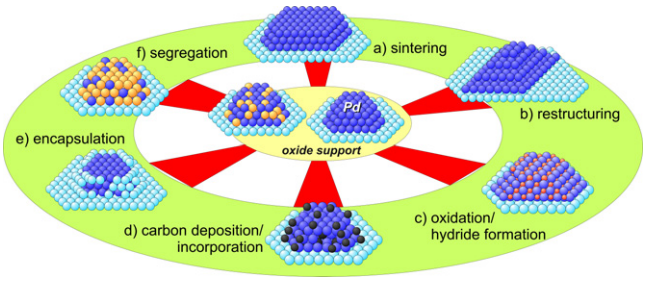

Figure 1. Illustration of structural and compositional changes that may occur during the transformation of catalysts from the 'as-prepared' to the 'active state': sintering and restructuring ((a), (b)), oxide/hydride formation and coking ((c), (d)), particle encapsulation (e) and surface segregation of bimetallic particles (see the text for details).

(ii) *Compositional changes.* Catalyst activation may also be performed by simply exposing the catalyst to reaction conditions. During the so called 'induction period' a stable activity is reached that may be higher or lower than the initial activity, paralleled by pronounced structural/compositional changes. For instance, Pd oxide phases [23, 24] and Pd hydrides [25–28] may be formed during oxidation and hydrogenation reactions, respectively (figure 1(c)). For hydrocarbon reactions the formation of carbonaceous species or of a metal–carbon phase (figure 1(d)) has been reported to be essential for high activity [29–34].

(iii) *Effects during catalyst lifetime.* After a catalyst has reached a stable initial activity it is still subject to mid- or long-term effects that typically reduce activity and/or negatively affect selectivity. For example, when rough (low-Miller-index) particle facets were produced during activation, long-term exposure to high reaction temperatures often re-establishes less active low-index facets [17, 35, 36]. This transformation may be assisted by the reaction gases, which weaken the metal–metal bonds (adsorbate-induced restructuring) [37]. For hydrocarbon (olefin, diene, or alkyne) hydrogenation carbon lay-down (coking) is a frequent cause of long-term deactivation, with the carbon species successively reducing the accessible catalyst (noble metal) area. For reducible support oxides, exposure to hydrogen leads to strong metal–support interaction (SMSI [21, 22]), manifest e.g. by particle encapsulation leading to deactivation (figure 1(e)). For bimetallic nanoparticles, the surface composition may change with time on-stream, e.g. due to the segregation of one constituent to the surface (figure 1(f)) [38–40], with pronounced influence on catalytic performance.

All of these effects have originally been established based on research on industrial-grade, chemically synthesized (powder) catalysts. Systematic studies varying the metal dispersion (particle size), support material and reaction conditions finally allowed suggestion of models and sometimes even mechanisms. The application of surface science methodology to heterogeneous catalysis was intended to unravel the origin of these effects *on a molecular level* and to improve existing catalysts. Early surface science applications to catalysis focused on the structure of clean single-crystal surfaces (relaxation and reconstruction) and their interaction with gas molecules (see e.g. [41–43] and references therein[2]). Soon after, single-crystal surfaces of various orientations [44, 45] were employed to examine structure sensitivity and metal–support interaction was tackled by depositing oxide overlayers on metal surfaces (inverse catalysts [19, 46]). Temperature-programmed desorption spectroscopy was extensively used to investigate gas–surface interactions (adsorption, coadsorption, reaction) on monometallic, bimetallic and oxide single crystals [47–49]. High-pressure cells, attached to ultrahigh-vacuum (UHV) surface analysis apparatus [50–52], were used to study reactions on single-crystal model catalysts at atmospheric pressure, with pre- and post-reaction surface analysis in UHV (only later on were *in situ* cells developed [53–56]; see below). Over the years, the focus shifted to nanoparticle model catalysts, examining particle nucleation and growth [13, 57–59], particle sintering [56], particle size effects, surface–gas interactions [60–62] and metal–support interaction [63–65]. Apparently, the UHV-based surface science approach to heterogeneous catalysis was quite successful in unraveling (elementary steps of) surface reactions, but the experimental conditions were typically very different from technological processes.

Therefore, substantial efforts have recently been devoted to developing a number of surface-sensitive methods that allow us to examine the evolution and transformation of active model catalyst phases under (near) ambient pressure (e.g. [23, 24, 28, 34, 61, 66–72]). One can now provocatively ask whether the fuzz about newly developed *in situ* high-pressure surface science is justified and not just 'a new twist to an old story'. However, as discussed below, there are several examples demonstrating that gas pressure indeed matters. One should also note that the classical models/explanations obtained from studies of technical catalysts, although often correct, were typically based on *indirect* evidence and suffered from the inability to characterize active structures on an atomic/molecular level (especially for complex porous catalysts). In the following, we illustrate how combining UHV-grown model catalysts with ambient pressure surface vibrational spectroscopy provides *direct* evidence and allows us to identify the nature and reactivity of specific adsorption sites, carbonaceous species, surface oxides and bimetallic ensembles, under conditions approaching those of technical applications. Photon-based methods such as polarization modulation infrared reflection absorption spectroscopy (PM-IRAS) and sum frequency generation (SFG) vibrational spectroscopy were utilized to monitor processes on well defined surfaces, including smooth and stepped single crystals, thin metal and oxide films, and oxide-supported nanoparticle model catalysts. Together with complementary information from high-pressure x-ray photoelectron spectroscopy (HP-XPS), mechanisms can be deduced on a molecular level. Microscopic studies revealed the restructuring of nanoparticles when exposed to reactive gases. *En route*, we discuss specific differences between UHV and high-pressure studies, as well as inherent differences between single crystals and

[2] Please note that the references in this paragraph are far from complete and are intended to direct the reader to the references cited in these articles.

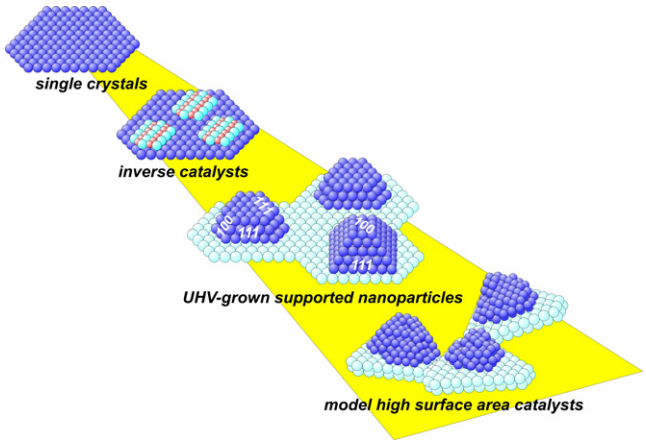

Figure 2. Model surfaces that have been utilized for studies of functioning catalysts at ambient pressure: (a) smooth and stepped noble metal single crystals, (b) thin oxide films grown on single-crystal substrates (inverse catalysts), (c) ultrahigh-vacuum-grown metal nanoparticles supported by thin oxide films (grown on single-crystal substrates) and (d) model high-surface-area catalysts. Systems (a)–(c) are prepared under ultrahigh vacuum, which allows control of catalyst morphology and composition (cleanliness). System (d) provides a link between surface-science-based and industrial catalysts.

nanoparticle model catalysts. The differences demonstrate the importance of 'minding the gap' between idealized and realistic conditions [67].

2. Planar model systems for metal oxide catalysts

Oxide-supported dispersed metals are widespread catalysts, such as the seemingly simple Pd–Al_2O_3, with Pd nanoparticles supported on a high-surface-area aluminum oxide (about 200 $m^2\ g^{-1}$). The Pd loading is often in the range of a few weight per cent or less, with a Pd particle diameter below ∼3 nm [73, 74]. The small particle size and the high-surface-area oxide make it typically very difficult to characterize or even detect the active metallic phase. Further complications may arise from oxide porosity and the presence of uncontrolled synthesis residues (which may either act as contaminants or promoters). Therefore, technological (industrial-grade) catalysts are often not well suited for atomic scale studies.

To overcome these limitations a variety of planar model catalysts has been developed [13, 18, 19, 58, 59, 61, 75–79] (figure 2). Many of them are prepared by evaporation methods under ultrahigh vacuum avoiding undesired contaminants and, due to their planarity and electrical/thermal conductivity, they are compatible with surface analytical methods. There are also preparation routes for clean model systems that are more similar to the technical catalyst preparation, for instance using 'residue-free' precursors [73], spin-coating [77, 80] or Langmuir–Blodgett methods [81], but these approaches will not be further discussed.

Single-crystal surfaces, although 'oversimplifying' a catalyst formulation, allow for ultimate control of surface structure and composition (figure 2). However, single crystals cannot mimic catalyst properties that originate from nanosize features or involve the oxide support. The next step towards supported metals was to use discontinuous thin oxide films, vacuum-grown on metal substrates, representing 'inverse catalysts' exhibiting metal/metal oxide phase boundaries [19, 46, 82, 83]. Probably the best models are metal nanoparticles grown on suitable oxide films (e.g. by physical vapor deposition of Pd) because they exhibit most important functionalities of a catalyst. Ideally, the oxide support should be an atomically flat and crystalline thin oxide film, facilitating the application of various spectroscopic/microscopic surface analysis techniques (due to the electrical/thermal conductivity of ultrathin oxide films). A number of well characterized thin oxide films has been developed, including Al_2O_3 grown on NiAl(110) [58, 78] or Ni_3Al(111) [84, 85], SiO_2 grown on Mo(112) [86–88], CeO_2 grown on Ru(0001) [89], Fe_3O_4 grown on Pt(111) [90, 91], MgO grown on Ag(100) [92], Nb_2O_5 grown on Cu_3Au(100) [93] etc (for a review see [94]). Appropriate control of the Pd deposition (evaporation amount and rate, substrate temperature, post-deposition processing) then allows growth of polyhedral Pd nanoparticles, such as the ones shown in figure 2, being truncated cuboctahedra exhibiting mostly (111) and (100) surface facets. Such particles are a nearly perfect test structure for fundamental studies (for scanning tunneling microscopy (STM) images cf figure 4 and see e.g. [58, 95–97]). Similarly, metal nanoparticles of other catalytically active materials (Pt, Rh, Ir, Ag, Au etc) and bimetallic nanoparticles can be prepared [66, 97–100]. To allow for control of interparticle distance, electron beam lithography has been applied to fabricate nanoparticle arrays on SiO_2 and Al_2O_3 films [101–105]. 'Model high-surface-area catalysts' of reduced complexity and with well defined structure/composition (figure 2) have also been applied for fundamental studies [73, 74, 106–110], but will not be further discussed here.

3. Vibrational spectroscopy on model catalysts at ambient pressure

The pretreatment-induced and reaction-induced transformations of a catalyst strongly depend on the exact conditions of gas pressure (O_2, H_2, reactants), temperature, time on stream etc, and, furthermore, the resulting phases and structures may be metastable. This means that an 'active phase' may only be present *under reaction conditions* while the catalyst functions, whereas pre- and post-reaction examination would often miss the relevant characteristics [111–113]. How much can one learn about a tennis match from just seeing two still photographs of the court taken before and after the match? Consequently, *in situ* examination is required, which has recently been termed *operando*, to more specifically refer to the need of simultaneous *spectroscopic and kinetic* measurements [114–116]. Such studies of 'catalysts at work' require surface spectroscopic methods that maintain their surface specificity at pressures in the mbar to >1 bar range [113]. Clearly, this can only be achieved when a spectroscopic method is either inherently surface specific (with no sensitivity to the

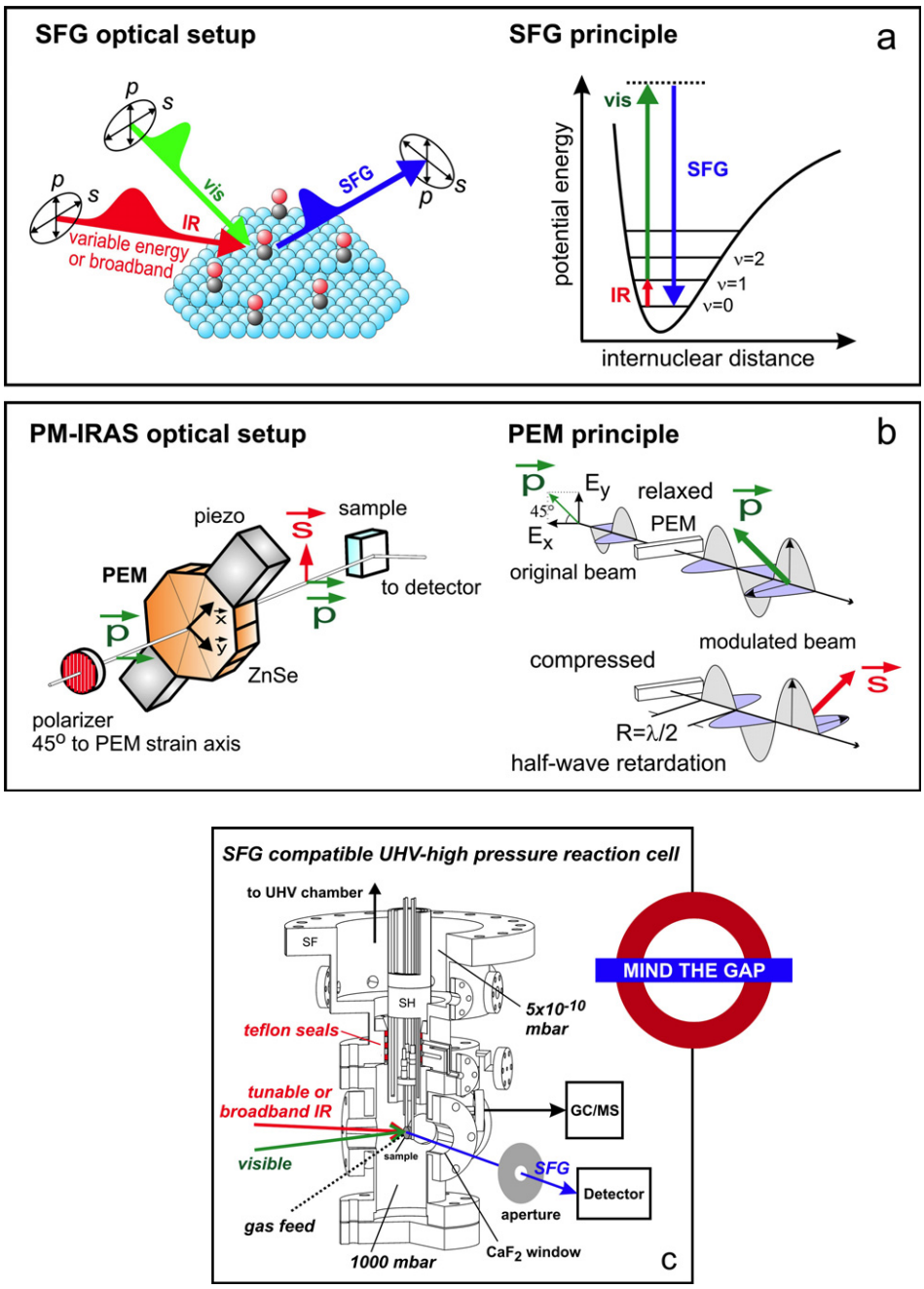

Figure 3. Illustration of surface vibrational spectroscopy by (a) IR–vis sum frequency generation (SFG) and (b) polarization-modulation infrared reflection absorption spectroscopy (PM-IRAS). Both methods are capable of monitoring molecules on surfaces under ambient pressure (mbar to >1 bar range). In (c) a high-pressure reaction cell for *in situ* optical spectroscopy on model catalysts is shown in cross section: sample holder (SH) and sealing flange (SF), housing three differentially pumped spring-loaded Teflon seals. The cell is coupled to an ultrahigh-vacuum (UHV) sample preparation and analysis system (not displayed). A single crystal is mounted on the sample holder, which is inserted into the Teflon seals. Adapted in part with permission from [141]. Copyright (2001) the PCCP Owner Societies.

gas phase) or when surface and gas phase contributions can be differentiated. In the following we discuss two 'high-pressure'[3] vibrational methods that are based on these two concepts and specifically aim at bridging the pressure gap: sum frequency generation (SFG) spectroscopy and polarization modulation infrared reflection absorption spectroscopy (PM-IRAS). Both methods can be applied from UHV to ambient pressure and are thus able to interconnect surface science studies with applied heterogeneous catalysis (for an overview see [61]).

(i) Non-linear optical IR–vis sum frequency generation (SFG) vibrational spectroscopy makes use of the second-order nonlinear optical process of SFG. Details of SFG theory have been described in [61, 117–122]. To probe the vibrational modes of a surface species two (e.g. picosecond) laser pulses are overlapped in space and time on the sample surface (figure 3(a)). One incident beam is in the visible range at fixed

[3] By 'high-pressure' we refer to studies at pressures above 1 mbar exceeding by far the pressure of typical UHV investigations ($\sim 10^{-8}$–10^{-10} mbar).

frequency (ω_{vis}; e.g. green), whereas the second one is energy-tuned in the mid-IR region (ω_{IR}). In the case of a vibrational resonance of a molecule adsorbed at the surface–gas interface, the two light waves interact and generate a wave at the sum of their frequencies ($\omega_{SFG} = \omega_{IR} + \omega_{vis}$), resulting in a signal in the visible (e.g. blue) region. In a simplified picture one can envision a vibrational transition from the ground state to an excited state, followed by excitation to a higher-energy virtual state and relaxation through an anti-Stokes Raman process (cf the energy scheme in figure 3(a)). By tuning the IR wavelength (wavenumber) and monitoring the SFG intensity, an adsorbate vibrational spectrum is obtained (cf figure 4(a)). According to the applicable selection rules a vibrational mode must be simultaneously IR and Raman active to be SFG active. Therefore, SFG is not allowed in media with inversion symmetry, as in the centrosymmetric bulk of a noble metal or in the isotropic gas phase, but has a finite value at the catalyst–gas interface, where the inversion symmetry is broken. Because this nonlinear process produces only a small signal, high incident light intensities, i.e. pulsed lasers, are required. SFG spectrometers have been designed based on neodymium yttrium–aluminum garnet (Nd:YAG), titanium sapphire (Ti:Sa) or free-electron lasers. For details on the generation of tunable IR and visible radiation and on the detection of the SFG signal we refer to the references in [61]. Specifics of the application of SFG to nanoparticle model catalysts, such as the effect of particle size and gas pressure [123–125] on site population and (co)adsorbate phases [27, 28], support effects [65, 66, 126] and the origin of SFG intensity and lineshape [127], have been described elsewhere.

Apart from the method described so far (i.e. 'scanning' SFG), there are other modes of operation, such as femtosecond 'broadband' SFG [128] (allowing us to capture the whole SFG spectrum within a few laser shots), time-resolved 'pump–probe' SFG (after excitation of the surface with an intense laser 'pump' pulse, a time-delayed weak SFG 'probe' monitors changes in the vibrational properties [129]) and polarization-dependent SFG (providing information on molecular orientation) [130–134]. Although particularly time-resolved broadband SFG has great potential for catalytic studies, to our knowledge no such studies were performed at ambient pressure and we will thus focus on scanning SFG below.

(ii) In contrast to SFG, which is inherently interface specific, polarization-modulated infrared reflection absorption spectroscopy (PM-IRAS) yields surface vibrational spectra via an accurate subtraction of the gas phase contributions, utilizing the polarization modulation of the incident IR light (figure 3(b)). As described by the metal surface selection rule [135], the effective surface intensity of s-polarized infrared light on a metal surface is basically zero and no surface absorption occurs. Thus, IR spectra acquired in s polarization are identical to IR gas phase spectra. In contrast, IR spectra acquired in p polarization contain absorption contributions of both surface and gas phase species. Consequently, (p − s) spectra ('surface' plus 'gas phase' minus 'gas phase') represent the vibrational signature of the surface species.

Polarization modulation is performed by a photoelastic modulator (PEM; ZnSe; figure 3(b)). The PEM principle is based on the *photoelastic effect*, describing the birefringence of a mechanically stressed crystal as being proportional to the resulting strain [136, 137]. Thus, different linear polarizations of light passing through the PEM have slightly different speeds of translation. When the optical PEM element is relaxed, linearly polarized monochromatic light passes without changing its polarization (figure 3(b)). When the optical element is compressed (stretched), the horizontal polarization component (parallel to the modulator axis) travels slightly faster (slower) than the vertical component. The phase difference between the two components is called the retardation, R. When the peak retardation is set to one-half of the light wavelength (*half-wave retardation mode*; figure 3(b)), the PEM rotates the light polarization by 90°. The polarization of the light impinging on the sample can thus be switched with a frequency of 37 kHz between p and s polarizations. Because the two polarization states occur twice within each PEM oscillating cycle, the sampling frequency is 74 kHz. Consequently, the p (surface and gas phase) and s (gas phase) spectra are acquired nearly simultaneously. After demodulation of the signal, (p − s) spectra are obtained which characterize the vibrational signature of the surface species, whereas the s spectra characterize the corresponding gas phase absorption.

Compared to SFG, PM-IRAS offers several advantages. SFG is typically limited to wavenumbers higher than ∼1600 cm^{-1}, whereas the frequency range of PM-IRAS (ca. 800–4000 cm^{-1}) allows additional detection of deformation modes, fingerprinting signatures etc. The acquisition of PM-IRAS spectra takes a few minutes (for a scan of 800–4000 cm^{-1}), whereas SFG rather takes 15–20 min (for a sweep of 1800–2200 cm^{-1}). PM-IRAS additionally provides information on gas phase species. On the other hand, SFG can be carried out in time-resolved pump–probe mode (with picosecond or even higher resolution [130, 138, 139]), as well as in polarization-dependent mode [131, 134, 140], determining, for instance, the tilt angle of specific bonds. With respect to the limitations of the methods one has to confess that nonlinear optical laser-based SFG is typically not easy to operate, requires significant maintenance and is thus not a plug-and-play technique. For intensity analysis, normalization to the effective surface IR intensity is not straightforward [61], putting limits on quantitative analysis, and the resolution of SFG (∼5 cm^{-1}) is lower than that of IR. Polarization-modulated IRAS requires metallic substrates and its combination with vacuum IR spectrometers and UHV systems is technically demanding.

Nevertheless, both SFG and PM-IRAS have been applied to UHV-based model catalysts. In order to carry out ambient pressure spectroscopy, UHV-compatible high-pressure cells have been developed, optimized for the specific method [61]. Figure 3(c) displays a cross section of a reaction cell that is coupled to a UHV surface analysis system (not shown). After sample preparation/characterization in UHV the model catalyst is transferred, with the help of an $xyz\theta$ manipulator and still under UHV, to the reaction cell. During this operation the sample holder is inserted into an arrangement of three differentially pumped spring-loaded Teflon seals and

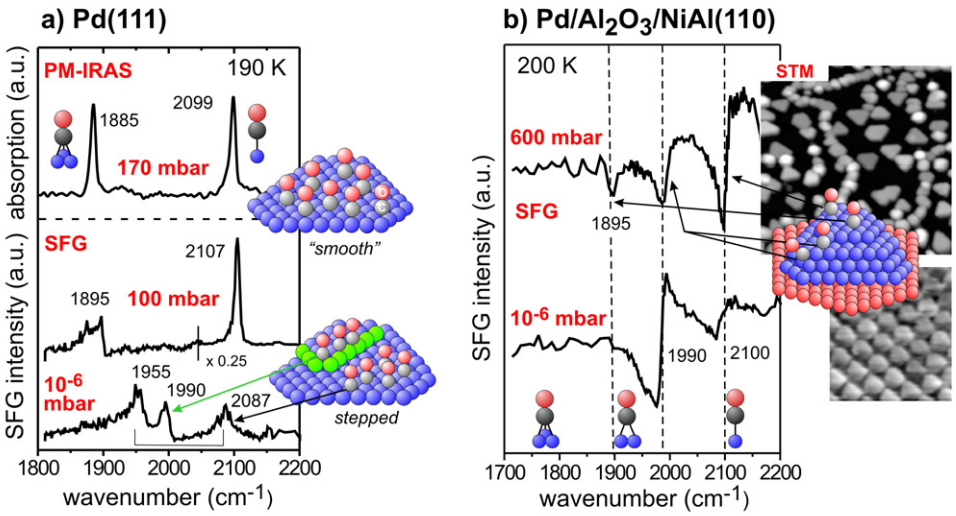

Figure 4. Vibrational SFG spectra of CO adsorption (10^{-6}–600 mbar) on (a) 'smooth' and stepped Pd(111), and (b) Pd nanoparticles supported by Al_2O_3 [28, 123–125]. The peaks characterizing the various binding geometries of CO on threefold hollow, bridge/edge and on-top Pd sites are indicated by arrows. Pronounced differences occur between Pd nanoparticles and single crystals, demonstrating the need to carry out model catalytic studies on supported nanoparticles. Adapted in part from [28, 125] with permission. Copyright (2002, 2005) Elsevier. The STM images of a Pd–Al_2O_3/NiAl(110) model catalyst in (c) illustrate the cuboctahedral shape of the Pd particles (upper image; 100×100 nm^2), and the (111) orientation of the particle top facet (lower image; 1.8×1.6 nm^2). Adapted from [97] with permission. Copyright (2007) Elsevier.

the reaction cell is separated from the UHV part [53, 61, 141]. Vibrational spectroscopy can then be performed in the reaction cell, either under UHV or at pressures up to 1 bar (the cell shown in figure 3 is designed for SFG but the arrangement for PM-IRAS is very similar). For catalytic tests, the SFG cell serves as a recirculated batch reactor and is interfaced to a gas chromatograph for product analysis. After the reaction, sample transfer under UHV back to the UHV analysis section allows for well controlled post-reaction surface characterization.

Vibrational spectroscopy alone may be insufficient to deduce reaction mechanisms, particularly when species with no or small IR activity are involved (such as carbonaceous or flat-lying species). Complementary methods are inevitable to provide information on catalyst structure and composition as well as on absolute adsorbate coverage. Consequently, SFG and PM-IRAS have been combined with (high-pressure) x-ray photoelectron spectroscopy [142–144]. HP-XPS confines the high-pressure region closely around the sample, using strong differential pumping of the sample compartment, x-ray source and electron energy analyzer [142, 143, 145–147]. Combined with synchrotron radiation that inherently carries higher resolution and allows us to increase surface sensitivity by using low photon energies (e.g. ∼650 eV instead of ∼1300 eV of a laboratory source), accurate composition characterization can be performed. HP-XPS will be discussed in the articles of Vass *et al* [148] and Yamamoto *et al* [149] in this issue.

4. Characterization of catalytically active phases under realistic conditions

Before turning to studies of catalytic surfaces under realistic conditions, one can ask what to expect from such studies. In figure 1 we have summarized some effects that can change the structure and composition of a catalytic material and, thus, reactivity. However, if we ignore these effects for a moment, is there a possibility that more fundamental high-pressure effects occur? For example, the molecular adsorbate geometries at ambient pressure could be significantly different from those observed under UHV at cryogenic temperatures. This would lead to a devastating difference between surface science and applied catalysis. However, no such unusual, unexpected high-pressure species have been observed. Nevertheless, there are still differences between UHV and ambient pressure studies but these are rather related to differences in the adsorbate surface concentration (coverage) and, thus, in the relative population of various sites. For example, for Pd surfaces hollow sites are preferred at low CO coverage whereas bridge and on-top sites are populated at higher coverage. Consequently, if the weakly bonded on-top CO or on-top H are essential for a reaction [27], the relevant species will only appear under catalytic conditions. One should note that high coverages can also be obtained under UHV at cryogenic temperatures, but the low temperature often produces kinetically trapped non-equilibrium adsorbate structures [150] that may favor different reaction routes. Such effects have been summarized as a 'pressure gap'. Similarly, the difference between noble metal single crystals and oxide-supported nanoparticles may have pronounced influence on catalytic performance, typically referred to as a 'materials gap' (including effects of geometric and electronic structure, metal–support interaction etc [58]). The complexity of industrial-grade catalysts often prevents fundamental studies and, furthermore, *exact* formulations may be a secret (and, at least on the atomic level, sometimes even unknown to the manufacturers). Therefore, researchers have tried to mimic technical systems as closely as possible and the

following examples are intended to provide an insight into how *in situ* spectroscopy on model systems helps in identifying the active phases of heterogeneous catalysts.

4.1. Adsorption and hydrogenation

The adsorption of CO is a prototypical test 'reaction' for the surface characterization of model catalysts. The huge efforts devoted to CO adsorption are justified by the involvement of CO in many important catalytic processes (methanol synthesis, Fischer–Tropsch, methanation, water gas shift, CO oxidation, etc [41, 151, 152]), and by its use as a probe molecule to 'titrate' the sites of a technological catalyst [153].

The relevance of surface science results for 'real world catalysts' has been questioned, but SFG and PM-IRAS can provide some answers. Figure 4 compares SFG and PM-IRAS spectra and shows the pressure dependence of CO adsorption on 'smooth' and stepped/ion-bombarded Pd(111), and on Pd nanoparticles (mean diameter ∼6 nm) supported by Al_2O_3/NiAl(110) [28, 58, 123]. At 10^{-6} mbar CO and 190 K, SFG detected bridging (1955 cm^{-1}) and on-top (∼2090 cm^{-1}) CO on Pd(111), but on stepped/ion-bombarded Pd(111) there was an additional peak at ∼1990 cm^{-1}, originating from CO adsorption on steps/defects (figure 4(a)). At high pressure (above 1 mbar), threefold hollow (∼1890 cm^{-1}) and on-top (∼2100 cm^{-1}) CO were observed both for 'smooth' and 'defect-rich' Pd(111), characterizing a (2 × 2) CO saturation structure (coverage 0.75 ML) [125, 154][4]. This does not indicate that the steps on the 'defect-rich' surface were removed by high-pressure CO (because this species reappeared upon decreasing the pressure), but rather indicates that on an extended single-crystal surface intermolecular coupling at high CO coverage no longer allows observation of the molecules adsorbed at step sites [124, 155].

Figure 4(b) shows corresponding SFG spectra for Pd nanoparticles. Based on the single-crystal measurements, IRAS spectroscopy [156] and density functional theory [157], the SFG peaks observed for Pd nanoparticles were assigned to CO adsorbed on threefold hollow sites (1895 cm^{-1}), bridge bonded CO at particle edges (1990 cm^{-1}) and particle terraces (shoulder at 1950 cm^{-1}) and to linearly (on-top) bonded CO (2100 cm^{-1}). The species are indicated in the figure and we refer to [61, 127] for a more detailed description of relative intensities and lineshapes. Apparently, there are differences between the high-pressure single-crystal and nanoparticle spectra. In particular, the band at 1990 cm^{-1}, characterizing CO at particle edges/steps, is absent at high pressure on Pd single crystals, whereas it is present for Pd nanoparticles. As mentioned, intermolecular CO coupling at high coverage obscures this species on an extended surface whereas on Pd nanoparticles such a 'masking' effect does not occur. In contrast, the edge bonded CO species is rather enhanced by intensity transfer from CO bound at the particle facets to edge-bonded CO [156]. Structure-induced differences between Pd nanoparticles and Pd single crystals also occurred for β-Pd hydride formation, because particle edges and steps facilitate the diffusion of surface hydrogen into the Pd bulk [27, 28]. This strongly suggests that, when possible, model studies should be performed on nanoparticle model catalysts.

4.2. Dehydrogenation

Selectivity, rather than activity, is the critical issue in catalysis, and the choice of a test reaction should account for this. Model studies involving methanol constitute a first step because CH_3OH exhibits different chemical bonds that can be activated. CH_3OH decomposition has two competing pathways: (i) dehydrogenation to give CO and H_2 (when the C–O bond stays intact) and (ii) C–O bond scission (cleavage of the C–O bond within a CH_yO species; $y = 1$–4) yielding carbonaceous deposits CH_x ($x = 0$–3) [66]. In the presence of oxygen, CH_3OH may be partially oxidized to produce formaldehyde CH_2O or fully oxidized to give CO_2.

Methanol decomposition and oxidation on noble metals are prototypical reactions with a large number of UHV studies reported (e.g. [144, 158–173]). In UHV, methanol was often adsorbed at low temperature and chemical changes upon annealing were monitored spectroscopically. This methodology is not representative for a technical catalytic reaction because under UHV CH_3OH may desorb (multilayer at 140 K, monolayer at 175 K) before it reacts, whereas for a high-pressure/high-temperature reaction the surface species are in equilibrium with the gas phase.

Figure 5 shows a selection of results that were obtained in a combined SFG, HP-XPS and PM-IRAS study of CH_3OH decomposition at elevated pressure [32, 144]. Upon exposing Pd(111) to 5 mbar CH_3OH at 300 K (figure 5(a)), PM-IRAS (p − s) surface spectra characterized all dehydrogenation intermediates, i.e. methoxy CH_3O (minute amounts around 2900 cm^{-1}; not shown; see figure 3(a) in [32]), formaldehyde CH_2O (ρCH_2 of formaldehyde in two different adsorption geometries at 1305 and 1255 cm^{-1} [174, 175][5]), and formyl CHO (CH bending or ν_{CO} at 1200 cm^{-1} [176]), beside adsorbed CO (νCO at ∼1840 cm^{-1}, typical of ∼0.3 ML coverage). HP-XPS at 0.1 mbar methanol at 300 K (figure 5(b); reaction time 150 min) indicated about 1 ML CH_x, pointing to significant methanolic C–O bond scission (CO and CH_xO cannot be differentiated, though). Under UHV, C–O bond scission typically does not occur on Pd(111), i.e. the *in situ* observation of CH_x again demonstrates that UHV results cannot necessarily be extrapolated to elevated pressures. A reaction pathway, like C–O bond scission, that may be a minor route under UHV, can become a dominating effect at elevated pressure.

To determine the nature of the CH_x species on Pd(111), the surface was saturated with CO at 90 K after the reaction, and an SFG spectrum was taken (not shown). Comparison with the corresponding CO-SFG spectrum of the clean Pd(111) surface indicated that the CH_x species mostly poisoned

[4] The small difference between the SFG and PM-IRAS spectra probably occurs from different contributions of CO domains with coverage lower than 0.75 [150].

[5] According to [174] formaldehyde is adsorbed in bridging and chelating geometry. A contribution of formate [175] cannot be excluded but will not be considered here.

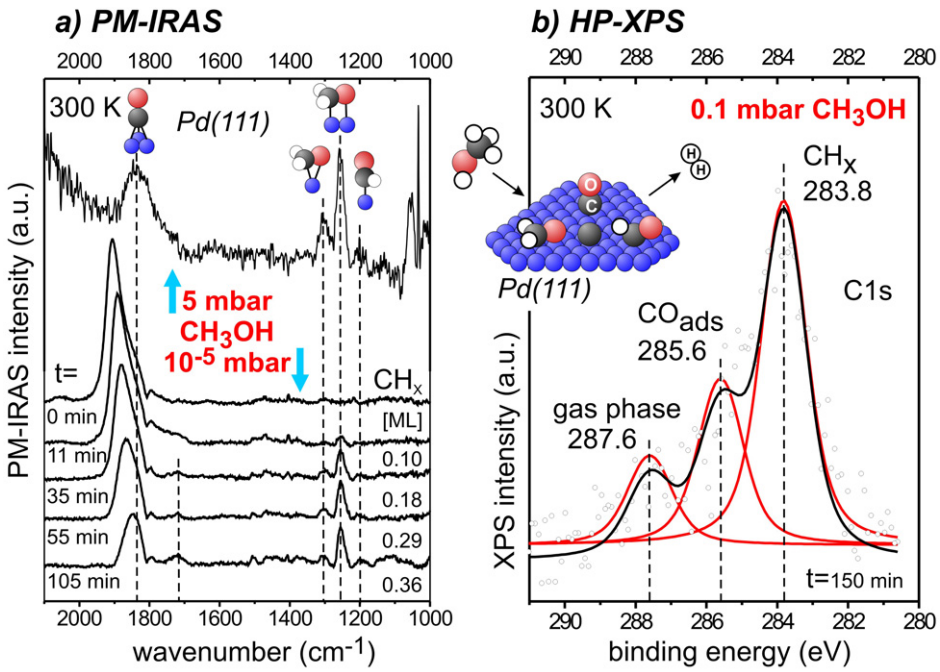

Figure 5. (a) PM-IRAS (p − s) surface vibrational spectra and (b) HP-XPS spectrum measured during CH_3OH decomposition on Pd(111) at 300 K, with the various species indicated. The time-dependent evolution of CH_2O (as observed by PM-IRAS) and of CH_x (values deduced from XPS) upon methanol decomposition at $\sim 10^{-5}$ mbar in (a) suggests a correlation between the two species. Adapted in part from [32] and [144] with permission. Copyright (2004, 2005) the American Chemical Society.

threefold hollow sites [144]. Taking into account the preferred tetravalency of carbon, CH_x is most likely atomic carbon and/or CH. It is now interesting to ask whether the CH_x species lower the activity simply by reducing the Pd surface area or whether they may also influence the reaction selectivity. Combined time-dependent PM-IRAS and XPS spectroscopy (figure 5(a)) has shown that the evolution of adsorbed CH_2O and of CH_x was correlated [32]. On a clean Pd surface CH_3OH decomposed to CO, whereas on a carbon-poisoned surface the amount of adsorbed CO decreased and more and more adsorbed CH_2O was observed, i.e. CH_x seems to 'stabilize' adsorbed CH_2O (cf CO and CH_2O peaks in figure 5(a); the CH_x coverage, as measured by XPS, is indicated). This can be rationalized considering that carbon adsorbed on threefold hollow sites hinders CH_2O dehydrogenation via HCO to CO by blocking the required (hollow) sites and CH_x may thus favor CH_2O formation (for details see [96]).

Carbon deposition on a catalyst surface (coking) is also observed during hydrocarbon hydrogenation/dehydrogenation reactions, originating from C–C bond scission and subsequent dehydrogenation. Apart from mere poisoning, it has been suggested that the carbon(aceous) species may be required to create the active site [30]. Alternatively, the local electronic structure may be changed [177]. Molecular beam studies of C_2H_4 dehydrogenation on Pd(110) and Pd(111) reported that carbon remains in the immediate subsurface region, with Pd acting as a carbon 'sponge' [31, 33]. Recent *in situ* XPS studies of alkene hydrogenation and oxidation on Pd single crystals, foil and nanoparticles even reported the formation of a new carbon phase (Pd_xC_y) under reaction conditions, which is very likely an active phase because activity was correlated with its occurrence [33, 68, 178].

4.3. Oxidation

As already mentioned, when oxygen is present in the feed gas, CH_3OH may be partially oxidized to produce formaldehyde CH_2O or fully oxidized to give CO_2. Pd nanoparticles (mean diameter 6 nm) supported on Al_2O_3/NiAl(110), as well as Pd(111), have also been utilized for studies of partial methanol oxidation [32, 61, 66, 179–181]. Under reactive conditions, when formaldehyde CH_2O, CO_2 and H_2O were produced, SFG and PM-IRAS detected hollow bonded CO as the only species on both types of palladium surfaces (figure 6(a)). Other reaction intermediates were too short lived for spectroscopic detection. However, CH_x species were observed even under oxidative conditions, and an influence on reactivity is again likely [32, 66]. Taking into account the stabilizing effect of CH_x on CH_2O described above, a clean surface should preferentially produce CO_2, whereas a partly CH_x-deactivated surface should additionally produce CH_2O, due to the hindered dehydrogenation of CH_2O [61]. In fact, at high reaction temperature (500 K) and low CH_x concentration ($\sim$0.1 ML) only CO_2 and water were produced, whereas at low reaction temperature (400 K) and high CH_x concentration ($\sim$0.4 ML) $\sim$20% CH_2O were observed [32].

The *in situ* studies also revealed a marked difference between Pd nanoparticles and single crystals: whereas Pd(111) remained metallic throughout the reaction at 400 K, post-reaction XPS indicated a significant oxidation of Pd particles

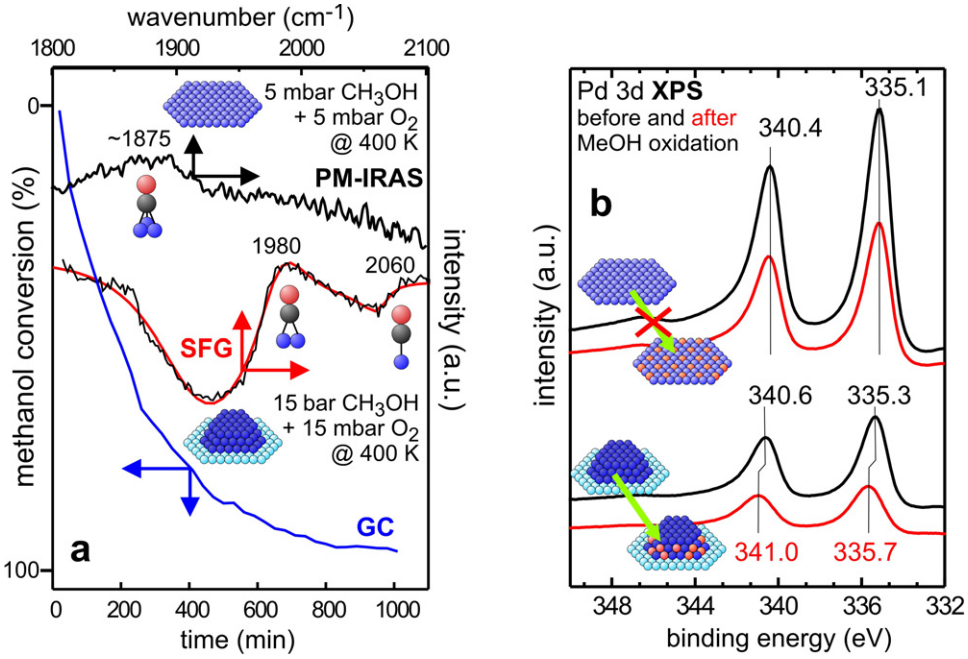

Figure 6. Methanol oxidation on Pd(111) and Pd–Al_2O_3 (mean particle size 6 nm) [32, 66, 181]. (a) *In situ* steady-state PM-IRAS and SFG spectra, shown together with the CH_3OH conversion as monitored by gas chromatography. (b) Comparison of Pd 3d XP spectra obtained before (upper) and after (lower) the methanol oxidation reaction indicated a partial oxidation of Pd nanoparticles during the reaction, whereas Pd(111) remained metallic. Adapted in part with permission from [66]. Copyright (2007) the PCCP Owner Societies.

during the high-pressure reaction (figure 6(b))[6]. This again points to the need to perform fundamental studies on realistic nanoscale models. The ∼0.4 eV binding energy shift observed by Pd 3d XPS for Pd particles indicates an oxidation state in between Pd and PdO, denoted here as PdO_x (the binding energy shift for PdO would be 1.5 eV [182]). Nevertheless, the observed vibrational frequencies of adsorbed CO were characteristic of metallic Pd, thus indicating a *partial* surface oxidation. Titration of the particle surface after the reaction using CO as probe molecule revealed that about 50% of the particle surface was oxidized [179]. Such partially oxidized Pd/PdO_x nanoparticles were investigated in detail by Schalow *et al* [183].

4.4. Activity of surface oxides

When oxidation reactions are carried out on noble metal catalysts, the concurrent oxidation of the metal itself has a major effect on catalytic activity. For example, for 'low temperature' (<1073 K) catalytic methane combustion on Pd–Al_2O_3 catalysts, PdO is considered the active phase [182, 184–186] (at higher temperature PdO decomposes and the reaction proceeds on metallic Pd). Demoulin *et al* [182] identified the PdO phase by *ex situ* XPS (indicating a Pd $3d_{5/2}$ binding energy (BE) of 336.2–336.5 eV) and by high-resolution transmission electron microscopy (HRTEM). However, the exact details of particle size and composition depend on metal loading, catalyst calcination, reaction conditions, and catalyst history in general.

[6] Because the catalysts were covered by CO after the reaction, the clean samples were also exposed to CO, responsible for the offset from 334.9 eV.

Figure 7(a) shows an HRTEM image of a 'fresh' 2% Pd–Al_2O_3 catalyst that had been heated in air to 873 K (3 h) (mean particle size 9.5 m). As a result, already before the CH_4 combustion reaction the particles were oxidized to PdO (XPS BE of ∼336.3 eV). In the technical catalysis literature such a catalyst is still named 'Pd–Al_2O_3', referring to the nominal composition of the (reduced) material, but this does not imply that researchers assume that the catalyst particles remain metallic Pd under oxidative reaction conditions.

It is also well known that a pre-oxidized CH_4 combustion catalyst further activates with time on stream. For example, under reaction conditions the conversion of 2% 'Pd–Al_2O_3' increased from ∼30% to ∼80% within 30 h [182]. During the activation period, particle sintering was observed (from 9.5 to 18.5 nm mean particle size) but also subtle changes in the Pd 3d BE (∼+0.2 eV) occurred that indicate a modification of the Pd oxide, paralleling the activity increase. Several reasons for the activation have been suggested, including the formation of specific PdO facets, changes of electronic structure due to changes in particle size, removal of contaminants, etc. Once an active PdO phase has been produced, the reaction temperature can be decreased by up to 100 K, maintaining the high activity. During the CH_4 combustion reaction, the PdO particles are continuously oxidized (by O_2) and reduced (by CH_4), creating a flexible structure with complex, varying PdO_x–PdO interfaces. After the 2% Pd–Al_2O_3 catalyst had been used at 825 K for 65 h, the restructuring produced regular polyhedral PdO particles (figure 7(b)). However, the *exact* structure and composition of the active phase, including the involvement of (sub)oxides other than PdO and of metallic Pd, can hardly be deduced from studies of industrial catalysts.

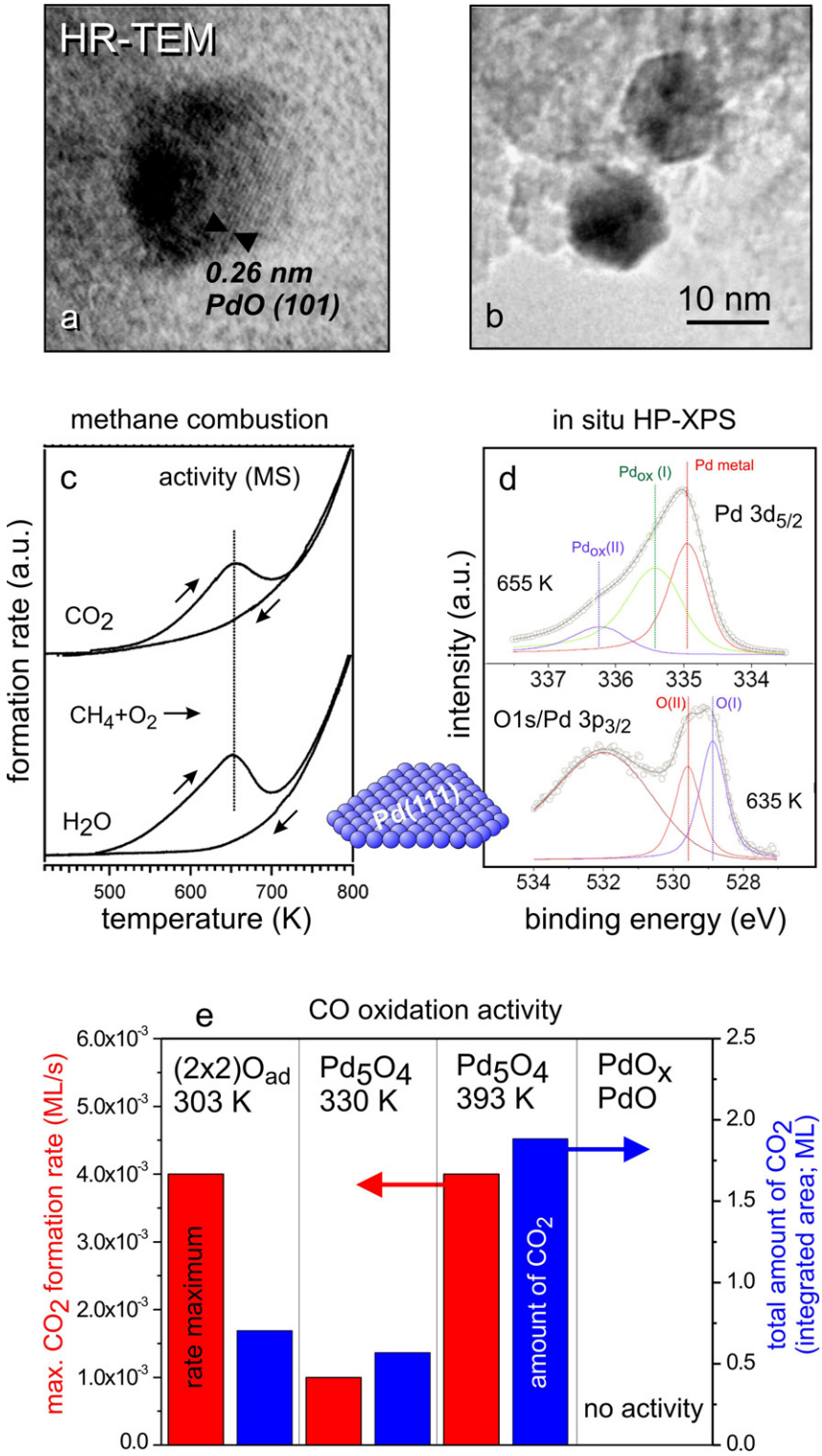

Figure 7. ((a), (b)) Transmission electron micrographs of an industrial 2 wt% 'Pd–Al_2O_3' catalyst used for methane combustion around 825 K. The lattice resolved image of a PdO nanoparticle is shown in (a), whereas faceted PdO nanoparticles that have been formed after long-term use are displayed in (b). ((c), (d)) *In situ* studies of CH_4 combustion on Pd(111), combining mass spectrometry and HP-XPS, suggest that the active phase consists of PdO seeds on a Pd_5O_4 surface oxide (see the text for details). Adapted in part from [69] with permission. Copyright (2007) the American Chemical Society. In (e), the CO oxidation activity of various Pd–O species, as determined by molecular beam and XPS studies [24], is compared (see the text for details).

As a consequence, intense research has recently been devoted to the characterization of Pd (surface) oxides [71, 187–189]. Gabasch *et al* and Ketteler *et al* have examined the oxidation of Pd(111) by *in situ* HP-XPS [24, 190–192]. Following the formation of the well known (2 × 2) chemisorbed oxygen adlayer, at an oxygen

pressure of 0.4 mbar a two-dimensional Pd_5O_4 surface oxide was observed above 470 K, transformed to PdO bulk oxide above 660 K, and PdO decomposed above 720 K. The stability range of the oxide phases was very sensitive to pressure and temperature, and a pronounced redox hysteresis was observed upon heating and cooling, in agreement with previous TEM studies [184]. Finally, a 'surface phase diagram' was reported for the O_2/palladium system, based on both experimental and theoretical investigations [71, 191]. For STM and XPS studies of the atomic structure of the two-dimensional Pd_5O_4 surface oxide we refer to [188].

After identifying the various Pd oxide species, synchrotron HP-XPS was applied to monitor CH_4 combustion on single-crystal Pd(111) (total pressure 0.3 mbar; CH_4:O_2 = 1:5) [69]. As shown in figures 7(c) and (d), there was a correlation between an activity maximum at 650 K and the presence of a surface phase consisting of PdO seeds on a Pd_5O_4 surface oxide[7]. The active phase is formed by a delicate balance of the formation of PdO seeds within Pd_5O_4 and the reduction of PdO by methane. Below 650 K, the model catalyst is less active because the active phase has not yet (fully) developed. Above 650 K, the active phase decomposes, which reduces activity. Above ∼720 K, activity increases again, with the reaction proceeding on metallic Pd. Above 800 K, the catalyst is metallic, with the near-surface region saturated with dissolved oxygen.

The importance of the formation of this specific surface phase was illustrated by the activity hysteresis observed during heating/cooling cycles, similar to that reported for technical catalysts [184, 185, 193]. As seen in figure 7(c), the activity maximum does not occur when cooling the metallic catalyst from high to low temperature because the PdO seeds/Pd_5O_4 phase is not produced (related to the formation of a different (passivating) surface oxide that seems to hinder PdO nucleation; for details see [69]). This confirms but also significantly refines the current understanding of catalytic methane combustion.

When oxidation reactions are performed at much lower temperatures, say up to 450 K, PdO is not formed but other surface oxides may still be present. In fact, a number of experimental and theoretical studies of CO oxidation on noble metal single crystals have reported the involvement of metal oxide phases under these conditions. For CO oxidation around 450–500 K oxides have been proposed to be more active than the metals for Ru [194], Pt [195, 196], and Pd [70]. The oxidation of CO on Pd and Pd oxides of various oxidation states was thus examined by molecular beam reactive scattering and x-ray photoelectron spectroscopy [24, 197]. Figure 7(e) compares the maximum CO_2 formation rates (turnover frequencies) and the total amount of CO_2 produced, based on molecular beam experiments (CO beam flux 0.02 ML s^{-1}; exposure time 900 s; for experimental details see [24]). Compared to the reaction of CO with chemisorbed (2 × 2) oxygen, the Pd_5O_4 surface exhibited a four times lower (maximum) activity around 300 K. In order to obtain an equal activity, the Pd_5O_4 surface temperature needed to be increased by at least 100 K. In this case the total amount of CO_2 produced was about 2.5 times higher because the nominal oxygen coverage is 0.58 for Pd_5O_4 [188] but only 0.25 for chemisorbed oxygen. The Pd oxide serves as an oxygen reservoir but, nevertheless, the reaction rate of the oxide is lower. For higher Pd oxidation states, i.e. PdO_x (BE shift of +0.4 eV) and PdO, no activity was observed under low-pressure conditions (reduction of PdO by CO required a pressure of 10 mbar at 523 K) [24].

For partially oxidized Pd nanoparticles supported on Fe_3O_4 a strongly reduced CO oxidation activity was deduced from extensive molecular beam/XPS studies, that were also able to disentangle the rates of CO reacting with chemisorbed oxygen and with Pd oxide [183, 197]. For Pd nanoparticles the situation is quite complex, because (i) nanoparticles are more easily oxidized than single crystals, (ii) the extent of oxidation is particle size dependent, and (iii) there is a coexistence of Pd metal and Pd oxide, with the latter growing preferentially at the metal–support interface [66, 183]. Studies of the specific activity of noble metals and of their oxides will certainly remain a vivid field of research in the near future.

4.5. Surface oxide structure

Apart from their catalytic properties, the atomic structure of surface oxides is most interesting. High-resolution transmission electron microscopy (HRTEM) has been extensively applied in the 1990s to examine the oxidation and reduction of noble metal nanoparticles that occurs during activation/regeneration cycles and which has strong influence on catalytic performance (for Rh nanoparticles on alumina, silica and ceria see e.g. [5, 8, 15, 17, 198]). Based on results from HRTEM and selected area electron diffraction (SAED), that indicated that the observed oxides were different from the known bulk structures, it was concluded that the structure of a thin e.g. Rh surface oxide may differ from that of bulk Rh_2O_3 [17, 198].

Figure 8 shows results of an HRTEM investigation of the oxidation and reduction of a Rh–Al_2O_3 model catalyst. Rh nanoparticles were grown epitaxially on crystalline substrates (e.g. NaCl(100)) and were then embedded in an thin (25 nm) amorphous alumina film, before the metal oxide system was lifted off the substrate [14, 17]. The epitaxial growth produced pyramidal nanoparticles with (111) and (100) surface facets, with the particle edges aligned with respect to each other (figure 8(a)). This particle ordering leads to a 'single-crystal-like' diffraction pattern [17], even though several hundred particles contributed to the diffraction image (figure 8(b))[8]. The pyramidal or, more precisely, half-octahedral shape of the Rh nanoparticles was further confirmed by weak-beam dark-field imaging (inset in figure 8(a)) and HRTEM (figure 8(d)). About 20% of the particles had other regular morphologies (pentagonal, half-tetrahedral, multiply twinned, etc) but for further details on nanoparticle characterization we refer to [17, 199].

[7] For an explanation of the analysis of this phase, based on the XPS signatures and relative intensities of the differently coordinated Pd and oxygen atoms, we refer to [69, 188].

[8] The electron diffraction pattern is centrosymmetric so only half of the pattern is shown here.

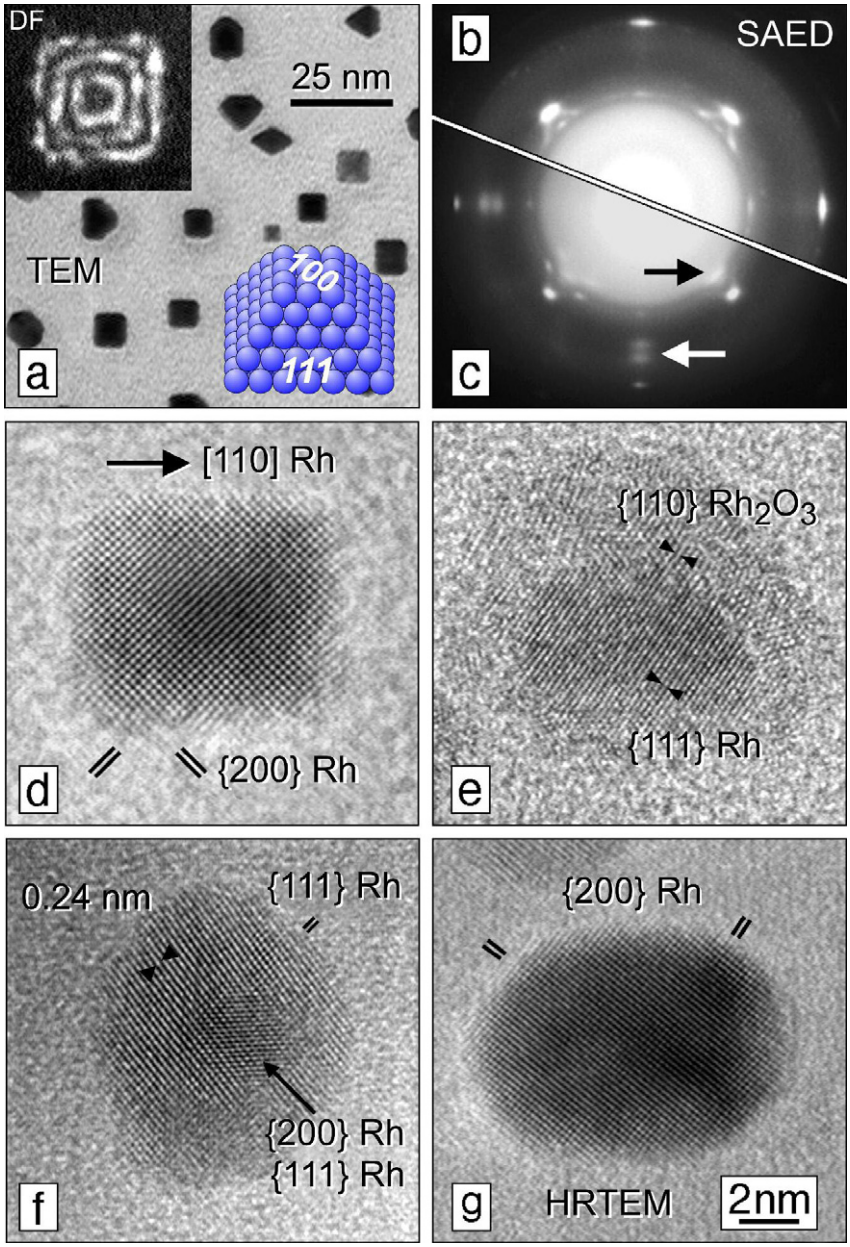

Figure 8. Oxidation and reduction of epitaxially grown polyhedral Rh nanoparticles on alumina (mean size 5 nm), monitored *ex situ* by HRTEM. In the as-prepared state, most of the Rh particles were half-octahedra with {111} and {100} surface facets, as revealed by combining results from HRTEM and WBDF ((a), (d)), and SAED (b). Upon oxidation in 1 bar O_2 at 723 K, an epitaxial Rh oxide shell developed on top of a Rh core ((c), (e)). Reduction in 1 bar H_2 at 523 and 723 K led to polycrystalline (f) and 'rounded' crystalline (g) nanoparticles, respectively. The microstructural changes were correlated with changes in catalytic hydrogenolysis activity (see text for details). Adapted in part from [17] with permission. Copyright (1998) Elsevier.

This model catalyst system provides a defined 'initial state' for studies of nanoparticle structure changes and has been applied to investigate the oxidation and reduction of Rh nanoparticles. Upon exposure to 1 bar O_2 at 725 K a Rh surface oxide was growing epitaxially on the metallic Rh core of the particles, as indicated by SAED. The oxide diffraction spots in figure 8(c), marked by arrows, were aligned with respect to the metal diffraction spots, revealing that the oxide grows epitaxially both on Rh(100) and Rh(111) particle facets [17, 198]. The formation of an epitaxial oxide was corroborated by HRTEM by imaging oxide lattice fringes of 0.26 nm spacing aligned nearly parallel to Rh{111}planes (spacing 0.22 nm; figure 8(e)). Based on the SAED and HRTEM results it was suggested that the structure of the oxide was related to hexagonal α-Rh_2O_3 but no perfect match was obtained. At the time the suggested structure was based on terminations of bulk Rh oxides, which, taking into account current knowledge [23], was doomed as a 'dead end'.

Upon reduction of the surface oxide in hydrogen at 523 K, rough (stepped) Rh particle facets were produced (figure 8(f)), due to the limited Rh diffusion at 523 K (the reduction temperature is too low for a recrystallization into perfect metal

nanoparticles [8]). The stepped Rh particle facets exhibited enhanced activity for hydrocarbon hydrogenolysis [17]. In addition, incomplete reduction of the Rh oxide layer produced rather complex Rh/Rh oxide/Rh sandwich structures. Only reduction at 723 K reestablished the well shaped single-crystalline Rh nanoparticles, at the expense of hydrogenolysis activity.

During the past years advanced surface imaging and surface spectroscopic methods (low-energy electron diffraction, STM, surface x-ray diffraction, photoemission) together with density functional theory (DFT) allowed researchers to resolve the structure of surface oxides grown on single-crystal substrates (for a review see [23]). For Rh, a hexagonal O–Rh–O trilayer on top of Rh(111) and Rh(100) has been observed. The surface oxide, with all octahedral sites of the oxygen lattice filled by Rh, differs from the Rh_2O_3 bulk structure, that has only two-thirds of the octahedral sites occupied by Rh. Similarly as for the oxidation of Rh nanoparticles discussed above, there was a defined orientation relationship between the surface oxide and the underlying metal. The characterization of surface oxides of Pd, Rh, Ru, Nb and other metals [23, 93, 94], that are different from truncations of bulk oxide structures, is a breakthrough in oxide surface chemistry. To extend the *in situ* studies to metal nanoparticles (e.g. [200, 201]), that simultaneously expose various surface facets, and to examine the effect of a support oxide (particle spreading; support wetting) is a challenge for the future. It may also be worthwhile to re-evaluate the existing HRTEM structure data on the oxidation of nanoparticles, taking into account the new knowledge on surface oxides.

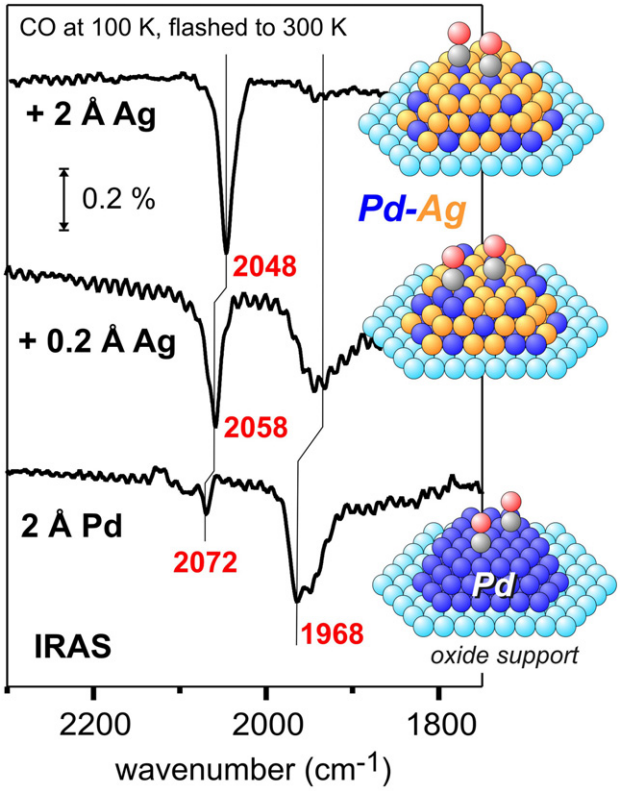

Figure 9. Infrared spectra of CO adsorbed on Pd and Pd–Ag nanoparticles. CO was adsorbed at 100 K and the samples were flashed to 300 K. The amount of Pd and Ag is given as nominal thickness (ångstrom). Addition of silver reduced the number of Pd bridge/threefold hollow sites (<1975 cm^{-1}) and thus favored adsorption on single Pd atoms (∼2050 cm^{-1}). Adapted from [100] with permission. Copyright (2006) Elsevier.

5. Approaching more complex systems means facing realistic problems

The progress in model catalysis and ambient pressure spectroscopy allow model studies to approach complex topics of applied catalysis. However, this is paralleled by also facing its problems. For example, when reducible oxides such as titania or niobia are used, strong metal–support interaction may occur. When Pd nanoparticles (mean diameter 3.5 nm) were supported on a thin (0.4 nm) Nb_2O_5 film on $Cu_3Au(100)$ [65, 93, 202], annealing already above 300 K induced strong structural changes. Combined TPD/SFG studies indicated that about 50% of the CO adsorption capacity was lost, that the maximum of desorption was shifted ∼250 K to lower temperature, and that 'mixed (alloyed) Pd–NbO_x' sites were produced. Such mixed metal–NbO_x compounds have been proposed as key components of active Fischer–Tropsch catalysts [203] but the 'deactivation' of the model system somewhat limits its application.

Promoted (monometallic) catalysts and bimetallic catalysts are among the most interesting materials in technical catalysis. The properties of bimetallics are generally very different from those of the constituent metals and, furthermore, their structure can be quite complex (alloyed nanoparticles, core–shell nanoparticles, contacting neighboring monometallic particles, etc). For Pd-based catalysts, various bimetallic systems have been reported, including Pd–Au [204, 205], Pd–Ag [100], Pd–Co [66, 97, 99, 206], Pd–Ni [207], Pd–Sn [208], etc.

When Pd is alloyed with a second metal two effects may occur: (i) the 'dilution' of Pd surface atoms by the second metal, creating isolated Pd atoms, referred to as 'site isolation' or 'ensemble effect', and (ii) electronic structure changes accompanying the first effect. Both effects are clearly connected, but the geometric site isolation model is often sufficient to explain the catalytic properties. Figure 9 compares IRAS spectra of CO adsorbed on (monometallic) Pd particles and Pd–Ag bimetallic catalysts supported on Al_2O_3, as reported by Khan *et al* [100]. When more and more Ag is evaporated onto the Pd particle surface, the Ag atoms break up the ensembles of threefold hollow and bridge Pd sites and create isolated (single) Pd atoms. The isolated Pd sites can then be 'titrated' by CO adsorption (figure 9). With increasing Ag content, the number of multiply coordinated Pd sites is reduced (decreasing peak around 1965 cm^{-1}) and a higher fraction of CO binds linearly to single Pd atoms (peak around 2060 cm^{-1}). At 100 K, another adsorption band at ∼2160 cm^{-1} was observed by Khan *et al* [100], growing with Ag content, which most likely originated from CO adsorbed on electronically modified neighboring Ag or Pd atoms (one

should note that CO does not adsorb on pure Ag under these conditions). The electronic structure of the nanoparticles was clearly affected by alloying of Pd and Ag, as indicated by an XPS Ag 3d binding energy shift of +0.7 eV compared to pure Ag [100]. Isolated Pd atoms on the surface of bimetallic Pd–Ag nanoparticles are considered crucial for the selective hydrogenation of acetylene C_2H_2 to ethylene C_2H_4 (whereas further hydrogenation of C_2H_4 to ethane C_2H_6 is slow). As mentioned, under high-pressure reaction conditions bimetallic particles may behave dynamically and the surface composition may change. However, such effects have not been tackled to date for UHV-grown nanoparticles.

6. Synopsis

Combining planar model catalysts and ambient pressure *in situ* spectroscopy allows one to successively approach the conditions of technical catalysis. Considerable progress has been made with respect to the preparation of increasingly complex nanoparticle model catalysts, but the reactive environment may strongly change the structure and composition of the nanoparticles. The identification of the 'active phase' thus requires investigations to be carried out under realistic working conditions. Vibrational spectroscopy by SFG and PM-IRAS can be performed in a pressure range from ultrahigh vacuum to ambient conditions, maintaining the surface specificity. This makes these methods prime techniques for linking surface chemistry with nanocatalysis.

A number of case studies were presented to illustrate how to monitor a catalytically active surface. No new 'high-pressure' surface chemistry was observed, but the site populations under high-pressure conditions may be different from those observed under UHV. Reaction pathways that are of minor importance under UHV may strongly influence a reaction under technically more relevant conditions, as shown for methanolic C–O bond scission. Supported nanoparticles behave differently from single crystals, as discussed for CO adsorption and methanol oxidation. These differences are often due to structure effects, such as the presence of edge and step sites on nanoparticles, but may also be related to the 'finite size' of nanoparticles, that makes them more sensitive to oxidation, coking, hydride formation, etc. Even with stepped single crystals, such effects cannot be fully modeled.

The characterization of surface oxides on Pd and Rh nanoparticles/single crystals is a fascinating branch of interface science. Partial oxidation of metal nanoparticles may occur during oxidation reactions, and detailed studies of the specific activity of the metal and oxide phase are required to identify the (more) active phase. Ambient-pressure model studies of metal–support interaction, bimetallic nanoparticles and complex reactions that require effective control of selectivity have scarcely been tackled to date but will become a major research topic. When model catalysis approaches the conditions of applied catalysis, it also has to face realistic problems and will lose part of the structural control, which is counterintuitive, because the main benefit of model catalysis is that all parameters are well defined. So let's 'mind the gap' and see where the voyages of this enterprise will take us.

Acknowledgments

We are grateful to the colleagues whose names appear in the list of references, particularly to M Borasio, V I Bukhtiyarov, H-J Freund, H Gabasch, H Hofmeister, V V Kaichev, B Klötzer, M Morkel, R Schlögl, and H Unterhalt. The STM images in figure 4(c) are courtesy of E Napetschnig, M Schmid, and P Varga. Funding by the German Science Foundation through program SPP 1091 and the Austrian Academic Exchange Program is gratefully acknowledged.

References

[1] Wang T, Lee C and Schmidt L D 1985 *Surf. Sci.* **163** 181
[2] Gillet M and Renou A 1979 *Surf. Sci.* **90** 91
[3] Jefferson D A and Harris P J F 1988 *Nature* **332** 617
[4] Hayek K 1989 *J. Mol. Catal.* **51** 347
[5] Burkhardt J and Schmidt L D 1989 *J. Catal.* **116** 240
[6] Giorgio S, Henry C R and Chapon C 1990 *J. Cryst. Growth* **100** 254
[7] Schmidt L D and Krause K R 1992 *Catal. Today* **12** 1035
[8] Logan A D, Sharoudi K S and Datye A K 1991 *J. Phys. Chem.* **95** 5568
[9] Henry C R, Chapon C, Duriez C and Giorgio S 1991 *Surf. Sci.* **253** 177
[10] Datye A K and Smith D J 1992 *Catal. Rev. Sci. Eng.* **34** 129
[11] Poppa H 1993 *Catal. Rev. Sci. Eng.* **35** 359
[12] Giorgio S, Henry C R, Chapon C and Roucau C 1994 *J. Catal.* **148** 534
[13] Rupprechter G, Seeber G, Hayek K and Hofmeister H 1994 *Phys. Status Solidi* a **146** 449
[14] Rupprechter G, Hayek K, Rendón L and José-Yacamán M 1995 *Thin Solid Films* **260** 148
[15] Bernal S, Botana F J, Calvino J J and Pérez-Omil J A 1995 *Catal. Today* **23** 219
[16] José-Yacamán M, Díaz G and Gómez A 1995 *Catal. Today* **23** 161
[17] Rupprechter G, Hayek K and Hofmeister H 1998 *J. Catal.* **173** 409
[18] Henry C R 1998 *Surf. Sci. Rep.* **31** 235
[19] Hayek K, Fuchs M, Klötzer B, Reichl W and Rupprechter G 2000 *Top. Catal.* **13** 55
[20] Sushumna I and Ruckenstein E 1987 *J. Catal.* **108** 77
[21] Tauster S J, Fung S C and Garten R L 1978 *J. Am. Chem. Soc.* **100** 170
[22] Hayek K, Kramer R and Paal Z 1997 *Appl. Catal.* A **162** 1
[23] Lundgren E, Mikkelsen A, Andersen J N, Kresse G, Schmid M and Varga P 2006 *J. Phys.: Condens. Matter* **18** 481
[24] Gabasch H, Knop-Gericke A, Schlögl R, Borasio M, Weilach C, Rupprechter G, Penner S, Jenewein B, Hayek K and Klötzer B 2007 *Phys. Chem. Chem. Phys.* **9** 533
[25] Palczewska W 1975 *Adv. Catal.* **24** 245
[26] Ceyer S T 2001 *Acc. Chem. Res.* **34** 737
[27] Rupprechter G, Morkel M, Freund H-J and Hirschl R 2004 *Surf. Sci.* **554** 43
[28] Morkel M, Rupprechter G and Freund H-J 2005 *Surf. Sci. Lett.* **588** L209
[29] McNamara J, Jackson S and Lennon D 2003 *Catal. Today* **81** 583
[30] Kennedy D R, Webb G, Jackson S D and Lennon D 2004 *Appl. Catal.* A **259** 109
[31] Bowker M, Morgan C, Perkins N, Holroyd R P, Fourre E, Grillo F and MacDowall A 2005 *J. Phys. Chem.* B **109** 2377

[32] Borasio M, Rodríguez de la Fuente O, Rupprechter G and Freund H-J 2005 *J. Phys. Chem.* B **109** 17791
[33] Gabasch H, Hayek K, Klötzer B, Knop-Gericke A and Schlögl R 2006 *J. Phys. Chem.* B **110** 4947
[34] Teschner D *et al* 2006 *J. Catal.* **242** 26
[35] Rupprechter G and Freund H-J 2001 *Top. Catal.* **14** 3
[36] Ramachandran A S, Anderson S L and Datye A K 1993 *Ultramicroscopy* **51** 282
[37] Van Hove M A and Somorjai G A 1994 *Surf. Sci.* **299/300** 487
[38] Bloxham L H, Haq S, Jugnet Y, Bertolini J C and Raval R 2004 *J. Catal.* **227** 33
[39] Saint-Lager M C, Jugnet Y, Dolle P, Piccolo L, Baudoing-Savois R, Bertolini J C, Bailly A, Robach O, Walker C and Ferrer S 2005 *Surf. Sci.* **587** 229
[40] Caballero G E R and Balbuena P B 2006 *Mol. Simul.* **32** 297
[41] Somorjai G A 1994 *Introduction to Surface Chemistry and Catalysis* (New York: Wiley)
[42] Rupprechter G and Somorjai G A 2006 *Landolt–Börnstein: Physics of Covered Solid Surfaces* ed H P Bonzel (Berlin: Springer) p 243
[43] Ertl G 1994 *Surf. Sci.* **299/300** 742
[44] Davis S M, Zaera F and Somorjai G A 1982 *J. Am. Chem. Soc.* **104** 7453
[45] Goodman D W 1982 *Surf. Sci.* **123** L679
[46] Levin M E, Williams K J, Salmeron M, Bell A T and Somorjai G A 1988 *Surf. Sci.* **195** 2807
[47] Madix R J 1979 *Chemistry and Physics of Solid Surfaces* ed R Vanselow (Boca Raton, FL: CRC Press)
[48] Yates J T 1985 *Solid State Physics: Surfaces* ed R L Park and M G Lagally (New York: Academic)
[49] Madix R J 1994 *Surf. Sci.* **299/300** 785
[50] Cabrera A L, Spencer N D, Kozak E, Davies P W and Somorjai G A 1982 *Rev. Sci. Instrum.* **53** 1888
[51] Goodman D W, Kelley R D, Madey T E and Yates J T 1980 *J. Catal.* **63** 226
[52] Reichl W, Rosina G, Rupprechter G, Zimmermann C and Hayek K 2000 *Rev. Sci. Instrum.* **71** 1495
[53] Rupprechter G, Dellwig T, Unterhalt H and Freund H-J 2001 *Top. Catal.* **15** 19
[54] Kung K Y, Chen P, Wei F, Rupprechter G, Shen Y R and Somorjai G A 2001 *Rev. Sci. Instrum.* **72** 1806
[55] Lægsgaard E, Österlund L, Thostrup P, Rasmussen P B, Stensgaard I and Besenbacher F 2001 *Rev. Sci. Instrum.* **72** 3537
[56] Kolmakov A and Goodman D W 2003 *Rev. Sci. Instrum.* **74** 2444
[57] Bäumer M and Freund H-J 1999 *Prog. Surf. Sci.* **61** 127
[58] Freund H-J, Bäumer M and Kuhlenbeck H 2000 *Adv. Catal.* **45** 333
[59] Freund H-J, Bäumer M, Libuda J, Risse T, Rupprechter G and Shaikhutdinov S 2003 *J. Catal.* **216** 223
[60] Libuda J and Freund H-J 2005 *Surf. Sci. Rep.* **57** 157
[61] Rupprechter G 2007 *Adv. Catal.* **51** 133
[62] Ozensoy E and Goodman D W 2004 *Phys. Chem. Chem. Phys.* **6** 3765
[63] Stone P, Poulston S, Bennett R A and Bowker M 1998 *Chem. Commun.* 1369
[64] Dulub O, Hebenstreit W and Diebold U 2000 *Phys. Rev. Lett.* **84** 3646
[65] Höbel F, Bandara A, Rupprechter G and Freund H-J 2006 *Surf. Sci.* **600** 963
[66] Bäumer M, Libuda J, Neyman K M, Rösch N, Rupprechter G and Freund H-J 2007 *Phys. Chem. Chem. Phys.* **9** 3541
[67] Rupprechter G and Weilach C 2007 *Nano Today* **2** 20
[68] Gabasch H *et al* 2006 *J. Catal.* **242** 340
[69] Gabasch H *et al* 2007 *J. Phys. Chem.* C **111** 7957
[70] Hendriksen B L M, Bobaru S C and Frenken J W M 2005 *Catal. Today* **105** 234
[71] Lundgren E, Gustafson J, Mikkelsen A, Andersen J N, Stierle A, Dosch H, Todorova M, Rogal J, Reuter K and Scheffler M 2004 *Phys. Rev. Lett.* **92** 046101
[72] Costina I, Schmid M, Schiechl H, Gajdos M, Stierle A, Kumaragurubaran S, Hafner J, Dosch H and Varga P 2006 *Surf. Sci.* **600** 617
[73] Lear T, Marshall R, Gibson E K, Schütt T, Klapötke T M, Rupprechter G, Freund H-J, Winfield J M and Lennon D 2005 *Phys. Chem. Chem. Phys.* **7** 565
[74] Lear T, Marshall R, Lopez-Sanchez J A, Jackson S D, Klapötke T M, Bäumer M, Rupprechter G, Freund H-J and Lennon D 2005 *J. Chem. Phys.* **123** 174706
[75] Goodman D W 1995 *Chem. Rev.* **95** 523
[76] Somorjai G A 1996 *Chem. Rev.* **96** 1223
[77] Gunter P L J, Niemantsverdriet J W H, Ribeiro F H and Somorjai G A 1997 *Catal. Rev. Sci. Eng.* **39** 77
[78] Freund H-J 1997 *Angew. Chem. Int. Edn Engl.* **36** 452
[79] Campbell C T 1997 *Surf. Sci. Rep.* **27** 1
[80] Thüne P C, Loos J, Chen X, Kimmenade E M E v, Kong B and Niemantsverdriet J W 2007 *Top. Catal.* **46** 239
[81] Kweskin S J, Rioux R M, Habas S E, Komvopoulos K, Yang P and Somorjai G A 2006 *J. Phys. Chem.* B **110** 15920
[82] Surnev S, Kresse G, Ramsey M G and Netzer F P 2001 *Phys. Rev. Lett.* **87** 086102
[83] Schoiswohl J, Sock M, Chen Q, Thornton G, Kresse G, Ramsey M G, Surnev S and Netzer F P 2007 *Top. Catal.* **46** 137
[84] Degen S, Becker C and Wandelt K 2004 *Faraday Discuss.* **125** 343
[85] Hamm G, Barth C, Becker C, Wandelt K and Henry C R 2006 *Phys. Rev. Lett.* **97** 126106
[86] Schroeder T, Adelt M, Richter B, Naschitzki N, Bäumer M and Freund H-J 2000 *Surf. Rev. Lett.* **7** 7
[87] Chen M S, Santra A K and Goodman D W 2004 *Phys. Rev.* B **69** 155404
[88] Lu J-L, Kaya S, Weissenrieder J, Todorova T K, Sierka M, Sauer J, Gao H-J, Shaikhutdinov S and Freund H-J 2006 *Surf. Sci. Lett.* **600** L164
[89] Lu J-L, Gao H-J, Shaikhutdinov S and Freund H-J 2006 *Surf. Sci.* **600** 5004
[90] Weiss W and Schlögl R 2000 *Top. Catal.* **13** 75
[91] Lemire C, Meyer R, Heinrich V E, Shaikhutdinov S and Freund H-J 2004 *Surf. Sci.* **572** 103
[92] Sterrer M, Risse T, Pozzoni U M, Giordano L, Heyde M, Rust H P, Pacchioni G and Freund H-J 2007 *Phys. Rev. Lett.* **98** 096107
[93] Starr D E *et al* 2005 *Surf. Sci.* **599** 14
[94] Kuhlenbeck H and Freund H-J 2006 *Landolt–Börnstein: Physics of Covered Solid Surfaces* vol III-42 ed H P Bonzel (Berlin: Springer) p 332
[95] Højrup Hansen K, Worren T, Stempel S, Lægsgaard E, Bäumer M, Freund H-J, Besenbacher F and Stensgaard I 1999 *Phys. Rev. Lett.* **83** 4120
[96] Rupprechter G 2007 *Catal. Today* **126** 3
[97] Napetschnig E, Schmid M and Varga P 2007 *Surf. Sci.* **601** 3233
[98] Heemeier M, Carlsson A F, Naschitzki M, Schmal M, Bäumer M and Freund H-J 2002 *Angew. Chem. Int. Edn* **41** 4073
[99] Carlsson A F, Naschitzki M, Bäumer M and Freund H-J 2003 *J. Phys. Chem.* B **107** 778
[100] Khan N, Uhl A, Shaikhutdinov S K and Freund H-J 2006 *Surf. Sci.* **600** 1849
[101] Eppler A, Rupprechter G, Guczi L and Somorjai G A 1997 *J. Phys. Chem.* B **101** 9973

[102] Rupprechter G, Eppler A S, Avoyan A and Somorjai G A 2000 *Stud. Surf. Sci. Catal.* **130** 369
[103] Eppler A, Rupprechter G, Anderson E A and Somorjai G A 2000 *J. Phys. Chem.* B **104** 7286
[104] Avoyan A, Rupprechter G, Eppler A S and Somorjai G A 2000 *Top. Catal.* **10** 107
[105] Laurin M, Johanek V, Grant A W, Kasemo B, Libuda J and Freund H-J 2005 *J. Chem. Phys.* **123** 054701
[106] Bertarione S, Scarano D, Zecchina A, Johanek V, Hoffmann J, Schauermann S, Frank M, Libuda J, Rupprechter G and Freund H-J 2004 *J. Phys. Chem.* B **108** 3603
[107] Borchert H, Jürgens B, Zielasek V, Rupprechter G, Giorgio S, Henry C R and Bäumer M 2007 *J. Catal.* **247** 145
[108] Föttinger K, Schlögl R and Rupprechter G 2008 *Chem. Commun.* 320
[109] Thomas J M, Johnson B F G, Raja R, Sankar G and Midgley P A 2003 *Acc. Chem. Res.* **36** 20
[110] Sao-Joao S, Giorgio S, Penisson J, Chapon C, Bourgeois S and Henry C R 2005 *J. Phys. Chem.* B **109** 342
[111] Thomas J M and Somorjai G A (ed) 1999 *Top. Catal.* (Special issue on *in situ* characterization of catalysts)
[112] Schlögl R and Zecchina A (ed) 2001 *Top. Catal.* (Special issue on *in situ* characterization of catalysts)
[113] Knözinger H and Gates B C (ed) 2006/2007 *Adv. Catal.* **50–52**
[114] Guerrero-Perez M O and Banares M A 2002 *Chem. Commun.* 1292
[115] Weckhuysen B M 2003 *Phys. Chem. Chem. Phys.* **4** 4351
[116] Banares M A 2005 *Catal. Today* **100** 71
[117] Shen Y R 1989 *Nature* **337** 519
[118] Hall R B, Russell J N, Miragliotta J and Rabinowitz P R 1990 *Chemistry and Physics of Solid Surfaces* (*Springer Series in Surface Science*) ed R Vanselow and R Howe (Berlin: Springer) p 87
[119] Shen Y R 1994 *Surf. Sci.* **299/300** 551
[120] Somorjai G A and Rupprechter G 1999 *J. Phys. Chem.* B **103** 1623
[121] Williams C T and Beattie D A 2002 *Surf. Sci.* **500** 545
[122] Buck M and Himmelhaus M 2001 *J. Vac. Sci. Technol.* A **19** 2717
[123] Dellwig T, Rupprechter G, Unterhalt H and Freund H-J 2000 *Phys. Rev. Lett.* **85** 776
[124] Unterhalt H, Rupprechter G and Freund H-J 2002 *J. Phys. Chem.* B **106** 356
[125] Rupprechter G, Unterhalt H, Morkel M, Galletto P, Hu L and Freund H-J 2002 *Surf. Sci.* **502–503** 109
[126] Höbel F 2006 *PhD* Technical University Berlin, in preparation
[127] Morkel M, Unterhalt H, Klüner T, Rupprechter G and Freund H-J 2005 *Surf. Sci.* **586** 146
[128] Richter L T, Petrallimallow T P and Stephenson J C 1998 *Opt. Lett.* **23** 1594
[129] Hess C, Funk S, Bonn M, Denzler D N, Wolf M and Ertl G 2000 *Appl. Phys.* A **71** 477
[130] Bandara A, Kubota J, Onda K, Wada A, Kano S, Domen K and Hirose C 1998 *J. Phys. Chem.* B **102** 5951
[131] Bandara A, Dobashi S, Kubota J, Onda K, Wada A, Domen K, Hirose C and Kano S 1997 *Surf. Sci.* **387** 312
[132] Cremer P S, Su X, Somorjai G A and Shen Y R 1998 *J. Mol. Catal.* A **131** 225
[133] Volpp H-R and Wolfrum J 2001 *Applied Combustion Diagnostics* ed K Kohse-Höinghaus and J B Jeffries (New York: Taylor and Francis)
[134] Galletto P, Unterhalt H and Rupprechter G 2003 *Chem. Phys. Lett.* **367** 785
[135] Hoffmann F M 1983 *Surf. Sci. Rep.* **3** 103
[136] Hipps K W and Crosby G A 1979 *J. Phys. Chem.* **83** 555
[137] Barner B J, Green M J, Saez E I and Corn R M 1991 *Anal. Chem.* **63** 55
[138] Ueba H 1997 *Prog. Surf. Sci.* **55** 115
[139] Bonn M, Hess C, Funk S, Miners J, Persson B N J, Wolf M and Ertl G 2000 *Phys. Rev. Lett.* **84** 4653
[140] Metka U, Schweitzer M G, Volpp H R, Wolfrum J and Warnatz J 2000 *Z. Phys. Chem.* **214** 865
[141] Rupprechter G 2001 *Phys. Chem. Chem. Phys.* **3** 4621
[142] Kaichev V V, Prosvirin I P, Bukhtiyarov V I, Unterhalt H, Rupprechter G and Freund H-J 2003 *J. Phys. Chem.* B **107** 3522
[143] Rupprechter G, Kaichev V V, Unterhalt H, Morkel M and Bukhtiyarov V I 2004 *Appl. Surf. Sci.* **235** 26
[144] Morkel M, Kaichev V V, Rupprechter G, Freund H-J, Prosvirin I P and Bukhtiyarov V I 2004 *J. Phys. Chem.* B **108** 12955
[145] Ogletree D, Bluhm H, Lebedev G, Fadley C, Hussain Z and Salmeron M 2002 *Rev. Sci. Instrum.* **73** 3872
[146] Bluhm H, Hävecker M, Kleimenov E, Knop-Gericke A, Liskowski A, Schlögl R and Su D S 2003 *Top. Catal.* **23** 99
[147] Pantförder J, Pöllmann S, Zhu J F, Borgmann D, Denecke R and Steinrück H-P 2005 *Rev. Sci. Instrum.* **76** 014102
[148] Vass E M, Härecker M, Zafeiratos S, Teschner D, Knop-Gericke A and Schlögl R 2008 *J. Phys.: Condens. Matter* **20** 184016
[149] Yamamoto S, Bluhm H, Andersson K, Kelleler G, Ogasawara H, Salmeron M and Nilsson A 2008 *J. Phys.: Condens. Matter* **20** 184025
[150] Morkel M, Unterhalt H, Salmeron M, Rupprechter G and Freund H-J 2003 *Surf. Sci.* **532–535** 103
[151] Ertl G, Knözinger H and Weitkamp J 1997 *Handbook of Heterogeneous Catalysis* (Weinheim: VCH)
[152] Chorkendorff I and Niemantsverdriet J W 2003 *Concepts of Modern Catalysis and Kinetics* (Weinheim: Wiley–VCH)
[153] Gruber H L 1962 *J. Phys. Chem.* **66** 48
[154] Kuhn W K, Szanyi J and Goodman D W 1992 *Surf. Sci. Lett.* **274** L611
[155] Greenler R G and Brandt R K 1995 *Colloids Surf.* A **105** 19
[156] Wolter K, Seiferth O, Kuhlenbeck H, Bäumer M and Freund H-J 1998 *Surf. Sci.* **399** 190
[157] Yudanov I V *et al* 2003 *J. Phys. Chem.* B **107** 255
[158] Christmann K and Demuth J E 1982 *J. Chem. Phys.* **76** 6308
[159] Kok G A, Noordermeer A and Nieuwenhuys B E 1983 *Surf. Sci.* **135** 65
[160] Gates J A and Kesmodel L L 1983 *J. Catal.* **83** 437
[161] Guo X, Hanley L and Yates J T 1989 *J. Am. Chem. Soc.* **111** 3155
[162] Davis J L and Barteau M A 1990 *Surf. Sci.* **235** 235
[163] Francis S M, Corneille J, Goodman D W and Bowker M 1996 *Surf. Sci.* **364** 30
[164] Levis R J, Zhicheng J and Winograd N 1989 *J. Am. Chem. Soc.* **111** 4605
[165] Chen J-J, Jiang Z-C, Zhou Y, Chakraborty B R and Winograd N 1995 *Surf. Sci.* **328** 248
[166] Kruse N, Rebholz M, Matolin V, Chuah G K and Block J H 1990 *Surf. Sci.* **238** L457
[167] Rebholz M and Kruse N 1991 *J. Chem. Phys.* **95** 7745
[168] Schauermann S, Hoffmann J, Johánek V, Hartmann J, Libuda J and Freund H-J 2002 *Catal. Lett.* **84** 209
[169] Schennach R, Eichler A and Rendulic K D 2003 *J. Phys. Chem.* B **107** 2552
[170] Zhang C J and Hu P 2001 *J. Chem. Phys.* **115** 7182
[171] Mavrikakis M and Barteau M A 1998 *J. Mol. Catal.* A **131** 135
[172] Rodríguez de la Fuente O, Borasio M, Galletto P, Rupprechter G and Freund H-J 2004 *Surf. Sci.* **566–568** 740
[173] Schauermann S, Hoffmann J, Johánek V, Hartmann J, Libuda J and Freund H-J 2002 *Angew. Chem. Int. Edn* **41** 2532
[174] Barros R B, Garcia A R and Ihlarco L M 2001 *J. Phys. Chem.* B **105** 11186
[175] Endo M, Matsumoto T, Kubota J, Domen K and Hirose C 2001 *J. Phys. Chem.* B **105** 1573

[176] Mitchell W J, Xie J, Jachimowski T A and Weinberg W H 1995 *J. Am. Chem. Soc.* **117** 2606
[177] Stolbov S, Mehmood F, Rahman T S, Alatalo M, Makkonen I and Salo P 2004 *Phys. Rev.* B **70** 155410
[178] Teschner D, Pestryakov A, Kleimenov E, Havecker M, Bluhm H, Sauer H, Knop-Gericke A and Schlögl R 2005 *J. Catal.* **230** 195
[179] Borasio M 2006 *PhD Thesis* Free University Berlin
[180] Morkel M 2004 *PhD Thesis* Free University Berlin
[181] Rupprechter G, Unterhalt H, Borasio M, Morkel M and Freund H-J 2005 *Annu. Reports of the Max Planck Society (Jahrbuch)* p 193
[182] Demoulin O, Rupprechter G, Seunier I, Clef B L, Navez M and Ruiz P 2005 *J. Phys. Chem.* B **109** 20454
[183] Schalow T, Laurin M, Brandt B, Schauermann S, Guimond S, Kuhlenbeck H, Starr D E, Shaikhutdinov S K, Libuda J and Freund H-J 2005 *Angew. Chem. Int. Edn* **44** 7601
[184] Datye A K, Bravo J, Nelson T R, Atanasova P, Lyubovsky M and Pfefferle L 2000 *Appl. Catal.* A **198** 179
[185] Salomonsson P, Johansson S and Kasemo B 1995 *Catal. Lett.* **33** 1
[186] Zhang H, Gromek J, Augustine M, Fernando G, Rasamny M, Boorse R S and Marcus H L 2001 *Proc. Frict. Stir Weld. Process. Symp.* p 59
[187] Leisenberger F P, Koller G, Sock M, Surnev S, Ramsey M G, Netzer F P, Klötzer B and Hayek K 2000 *Surf. Sci.* **445** 380
[188] Lundgren E, Kresse G, Klein C, Borg M, Andersen J N, De Santis M, Gauthier Y, Konvicka C, Schmid M and Varga P 2002 *Phys. Rev. Lett.* **88** 246103
[189] Gabasch H, Unterberger W, Hayek K, Klötzer B, Kresse G, Klein C, Schmid M and Varga P 2005 *Surf. Sci.* **600** 205
[190] Gabasch H *et al* 2006 *Surf. Sci.* **600** 2980
[191] Ketteler G, Ogletree D F, Bluhm H, Liu H, Hebenstreit E L D and Salmeron M 2005 *J. Am. Chem. Soc.* **127** 18269
[192] Zemlyanov D *et al* 2006 *Surf. Sci.* **600** 983
[193] McCarty J G 1995 *Catal. Today* **26** 283
[194] Over H, Kim Y D, Seitsonen A P, Wendt S, Lundgren E, Schmid M, Varga P, Morgante A and Ertl G 2000 *Science* **287** 1474
[195] Hendriksen B L M and Frenken J W M 2002 *Phys. Rev. Lett.* **89** 046101
[196] Ackermann M D *et al* 2005 *Phys. Rev. Lett.* **95** 255505
[197] Schalow T, Brandt B, Laurin M, Schauermann S, Libuda J and Freund H-J 2006 *J. Catal.* **242** 58
[198] Logan A D, Braunschweig E J, Datye A K and Smith D J 1989 *Ultramicroscopy* **31** 132
[199] Rupprechter G, Hayek K and Hofmeister H 1995 *Vacuum* **46** 1035
[200] Giorgio S, Sao Joao S, Nitsche S, Chaudanson D, Sitja G and Henry C R 2006 *Ultramicroscopy* **106** 503
[201] Kasper N, Stierle A, Nolte P, Jin-Phillipp Y, Wagner T, Oteyza D G d and Dosch H 2006 *Surf. Sci.* **600** 2860
[202] Middeke J, Blum R-P, Hafemeister M and Niehus H 2005 *Surf. Sci.* **587** 219
[203] Mendes F M T, Perez C A C, Noronha F B and Schmal M 2005 *Catal. Today* **101** 45
[204] Chen M S, Kumar D, Yi C W and Goodman D W 2005 *Science* **310** 291
[205] Hamm G, Becker C and Henry C R 2006 *Nanotechnology* **17** 1943
[206] Carlsson A F, Bäumer M, Risse T and Freund H-J 2003 *J. Chem. Phys.* **119** 10885
[207] Bertolini J C and Jugnet Y 2002 *Surface Alloys and Alloy Surfaces* ed D P Woodruff (Amsterdam: Elsevier) p 404
[208] Hamm G, Schmidt T, Breitbach J, Franke D, Becker C and Wandelt K 2004 *Surf. Sci.* **562** 170